Behavioral/Cognitive

Multiplexed Representation of Itch and Mechanical and Thermal Sensation in the Primary Somatosensory Cortex

Xiao-Jun Chen,[1,2] Yan-He Liu,[1,2] Ning-Long Xu,[1,2,3] and Yan-Gang Sun[1,3]

[1]Institute of Neuroscience, State Key Laboratory of Neuroscience, Center for Excellence in Brain Science & Intelligence Technology, Chinese Academy of Sciences, Shanghai, 200031, China, [2]University of Chinese Academy of Sciences, Beijing, 100049, China, and [3]Shanghai Center for Brain Science and Brain-Inspired Intelligence Technology, Shanghai, 201210, China

The primary somatosensory cortex (S1) plays a critical role in processing multiple somatosensations, but the mechanism underlying the representation of different submodalities of somatosensation in S1 remains unclear. Using *in vivo* two-photon calcium imaging that simultaneously monitors hundreds of layer 2/3 pyramidal S1 neurons of awake male mice, we examined neuronal responses triggered by mechanical, thermal, or pruritic stimuli. We found that mechanical, thermal, and pruritic stimuli activated largely overlapping neuronal populations in the same somatotopic S1 subregion. Population decoding analysis revealed that the local neuronal population in S1 encoded sufficient information to distinguish different somatosensory submodalities. Although multimodal S1 neurons responding to multiple types of stimuli exhibited no spatial clustering, S1 neurons preferring mechanical and thermal stimuli tended to show local clustering. These findings demonstrated the coding scheme of different submodalities of somatosensation in S1, paving the way for a deeper understanding of the processing and integration of multimodal somatosensory information in the cortex.

Key words: **itch; population coding; primary somatosensory cortex; sensory submodality; somatosensation; two-photon calcium imaging**

Significance Statement

Cortical processing of somatosensory information is one of the most fundamental aspects in cognitive neuroscience. Previous studies mainly focused on mechanical sensory processing within the rodent whisking system, but mechanisms underlying the coding of multiple somatosensations remain largely unknown. In this study, we examined the representation of mechanical, thermal, and pruritic stimuli in S1 by *in vivo* two-photon calcium imaging of awake mice. We revealed a multiplexed representation for multiple somatosensory stimuli in S1 and demonstrated that the activity of a small population of S1 neurons is capable of decoding different somatosensory submodalities. Our results elucidate the coding mechanism for multiple somatosensations in S1 and provide new insights that improve the present understanding of how the brain processes multimodal sensory information.

Introduction

Somatosensation is crucial for many physiological processes. It includes many different submodalities, and many efforts have been made to decipher the coding mechanisms of multiple submodalities of somatosensation. Previous studies found that a great proportion of DRG neurons responded to multiple types of stimuli, including mechanical, thermal, and chemical stimuli (Han et al., 2013; Wang et al., 2018; Paricio-Montesinos et al., 2020). In contrast, other studies reported that the vast majority of peripheral sensory neurons selectively responded to either heating or cooling stimuli (Yarmolinsky et al., 2016) and that mechanosensitive DRG neurons were not activated by various thermal stimuli (Emery et al., 2016). These data suggest that primary sensory afferents exhibit complicated response patterns to different somatosensory stimuli. In the spinal cord, it has been found that multiple somatosensory stimuli, including thermal, mechanical, pruritic, and nociceptive stimuli, could activate the same spinal neuronal population (Carstens, 1997; Davidson et al., 2007; Hachisuka et al., 2016; Ran et al., 2016). However, a previous study claimed the existence of a subset of spinothalamic tract neurons that were specifically involved in itch-related

Received July 13, 2021; revised Oct. 14, 2021; accepted Oct. 15, 2021.

Author contributions: X.-J.C., N.-L.X., and Y.-G.S. designed research; X.-J.C. performed research; X.-J.C. and Y.-H.L. analyzed data; X.-J.C., Y.-H.L., and Y.-G.S. wrote the paper; N.-L.X. and Y.-G.S. edited the paper.

This work was supported by National Natural Science Foundation of China 61890952 and 31771158; Shanghai Municipal Science and Technology Major Project Grant 2018SHZDZX05; and Strategic Priority Research Program of the Chinese Academy of Sciences Grant XDB32010200. We thank Drs. Robert H. LaMotte and Mu-Ming Poo for comments on the manuscript; Yan-Jing Zhu and Tong-Yu Liang for technical support; and all the members of the Y.-G.S. laboratory for helpful discussions.

The authors declare no competing financial interests.

Correspondence should be addressed to Yan-Gang Sun at yangang.sun@ion.ac.cn or Ning-Long Xu at xunl@ion.ac.cn.

https://doi.org/10.1523/JNEUROSCI.1445-21.2021

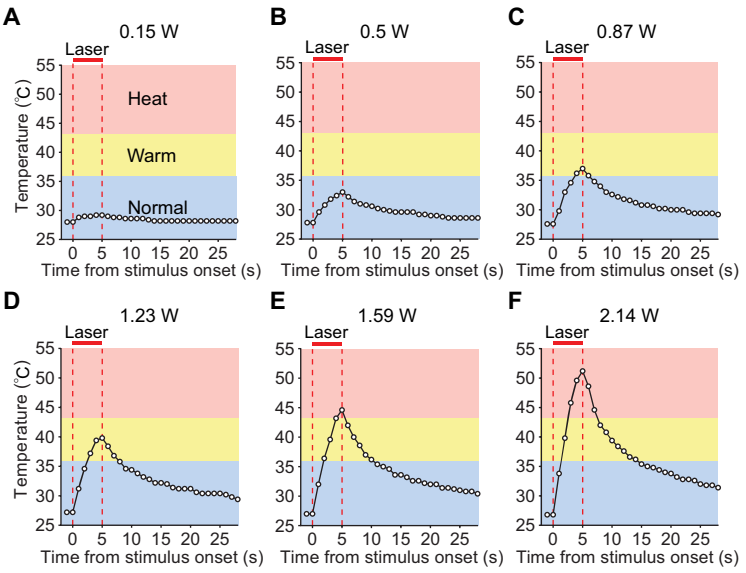

Figure 1. Measurement of skin temperature in response to infrared laser (976 nm)-based thermal stimuli. ***A-F***, Curves of the subcutaneous temperature measured with a thermometer probe under exposure to an infrared laser emitter with different levels of power. The optic fiber tip was placed at a distance of ~1.5 cm from the skin. Vertical dashed lines indicate laser stimulus onset and offset. Red bars represent the laser stimulation period.

signaling (Andrew and Craig, 2001), further raising the question of how the CNS decodes multiple submodalities of somatosensation.

It is generally believed that the perceptual distinction of different somatosensory submodalities is achieved at the cortical level (Ikoma et al., 2006; Dong and Dong, 2018); accordingly, the somatosensory cortex is the main focus for investigating the processing of somatosensory information. Previous macroscopic brain imaging and electrophysiological recording experiments have characterized responses in the primary somatosensory cortex (S1) to different types of stimuli and found that different submodalities of somatosensory stimuli evoked comparable activation in S1 (Mancini et al., 2012; Papoiu et al., 2012; Milenkovic et al., 2014; Khasabov et al., 2020). However, these studies either lack single-cell resolution or are limited by the relatively small number of recorded neurons; thus, how somatosensory information of multiple submodalities is decoded by the S1 population at the single-neuron level remains largely unknown. Population imaging provides us with the advantage of simultaneous recording of an unbiased large number of neurons, and these studies in S1 mainly focused on tactile information processing in the vibrissal system (Kerr et al., 2007; Chen et al., 2013a; Peron et al., 2015; Isett et al., 2018; Petersen, 2019; Brown et al., 2021). However, much less is known about how the S1 neuronal population processes other important submodalities of somatosensory information beyond the whisking system, such as pruritic and thermal sensation, in awake animals. Thus, it remains undetermined how S1 encodes and decodes different submodalities of somatosensation. Here, we examined the coding of mechanical, thermal, and pruritic stimuli in S1 by *in vivo* two-photon calcium imaging. We revealed a multiplexed representation for multiple somatosensory submodalities in S1 and demonstrated that the activity of a small population of S1 neurons is capable of decoding different somatosensory submodalities.

Materials and Methods

Animals. Male adult (7-14 weeks of age) C57BL/6N and *GRPR-iCreER* mice were used in all behavioral and imaging experiments. C57BL/6N WT mice were purchased from the SLAC laboratory (Shanghai). The generation of *GRPR-iCreER* mice has been described previously (Mu et al., 2017). All mice were housed on a 12 h light-dark cycle (lights on at 7:00 A.M.) with *ad libitum* food and water. All procedures were approved by the Animal Care and Use Committee of the Center for Excellence in Brain Science & Intelligence Technology, Chinese Academy of Sciences, Shanghai, China.

Surgeries. Mice were anesthetized with sodium pentobarbital solution (100 mg/kg body weight, i.p.) for all surgeries, and the body temperature was maintained at 37°C using a heating pad (RWD Life Sciences). Ophthalmic ointment was applied to the animals' eyes to maintain lubrication. All injections were performed using a picospritzer system controlled by a Master-8 stimulator (A.M.P.I.). Mice were allowed to recover from anesthesia on a heating blanket before being returned to their home cage. Mice were allowed to recover for at least 2 weeks before experiments.

Intraspinal cord injection. This procedure has been described previously (Mu et al., 2017). Briefly, paravertebral muscles and other tissues were retracted at vertebral levels C1-C5, and the exposed vertebral column was mounted and fixed on a stereotaxic apparatus. One segment of vertebral bone (C2 or C3) was removed, and a small incision was made on the dura for smooth penetration of the injection pipette. AAV-hSyn-Flex-ChrimsonR-tdTomato (AAV2/9, titer: 3.7×10^{12} vg/ml) or AAV-hSyn-DIO-mCherry (AAV2/9, titer: 3.0×10^{12} vg/ml) was injected into the right side of the spinal cord at 3 or 4 injection sites (interspaced by 400-500 μm, 400 nl per site) with a glass pipette targeted at the superficial dorsal horn. The pipette was withdrawn 5 min after virus injection.

LED implantation. For mice used in spinal optogenetics experiments, an LED (630 nm, Teleopto) was placed above the virus injection area of the exposed spinal cord and was stabilized with 3M Vetbond and dental cement. The surrounding skin was closed with stitches to provide better stability.

Chronic imaging window implantation. A circular craniotomy (~3 mm in diameter) was performed over the left S1Tr (center coordinate: AP 1.45 mm; ML 1.85 mm) or S1BF (center coordinate: AP 1.45 mm; ML 3.05 mm), and the dura was left intact. AAV-CaMKII-GCaMP6s (AAV2/9, titer: 1.2×10^{13} vg/ml) was slowly injected (200 nl per site, 2 sites interspaced by 250 μm; ~400 μm beneath the cortical surface) into the cortex. The injection pipette was withdrawn 5 min after the injection. An imaging window constructed with two glass coverslips (inner layer diameter ~2.5 mm, outer layer diameter ~5 mm) joined with an ultraviolet curable optical glue was inserted into the craniotomy area and sealed in place with dental cement. A titanium head plate with an opening in the middle was then attached to the skull with 3M Vetbond and dental dement to permit stable head fixation and two-photon imaging over the cranial window.

Tamoxifen injection. Tamoxifen was dissolved in sunflower oil at a concentration of 20 mg/ml and was injected into *GRPR-iCreER* mice at a dose of 150 mg/kg (i.p.) body weight for 5 consecutive days after virus injection.

Itch behavioral test. To measure scratching behavior, a small (1 mm in diameter, 3-mm-long cylinder) magnet was implanted into the back of the right hindpaw of each mouse. Their scratching behavior was recorded with a magnetic induction method as described previously (Mu et al., 2017). For optogenetic stimulation, the stimulus was delivered through a wireless optogenetic system (Teleopto) or a custom-made wire connected to a Master-9 stimulator. Adjustment of light frequency and LED output power was achieved by the Master-9 stimulator in wired mode. The scratching behavior of all mice used in opto-itch stimulation was measured before the imaging experiments.

Post hoc *histology*. After the imaging experiments were finished, the mice underwent histologic evaluation. This procedure has been described previously (Gao et al., 2019). Briefly, mice were anesthetized and perfused transcardially with 4% PFA (Sigma) solution. LEDs and head plates were retrieved for recycling use. Spinal cords and brains were dissected, post-fixed overnight at 4°C in 4% PFA, and then cryoprotected in 30% sucrose in PBS at 4°C. Free-floating sections (40 μm) were prepared using a Leica Microsystems CM 1950 cryostat. Images were taken using an Olympus VS120 fluorescence microscope.

In vivo *two-photon calcium imaging*. GCaMP6s was excited at 920 nm with a Ti: sapphire laser (Mai Tai, Spectra Physics) and imaged through a Nikon 16×, 0.8 NA water-immersion objective. Images (512 × 512 pixels, 420 × 423 μm) were acquired at ~ 30.9 Hz using National Instruments software. Before imaging, a particular FOV with strong GCaMP fluorescence was selected by adjusting the imaging plane (typically 130-170 μm below the cortical surface), and the same FOV was targeted in each session across different days based on vascular landmarks and visual comparison with previous images. To eliminate potential confounds from body movement-induced neuronal activity, mice were treated with chlorprothixene (2 mg/kg, i.m.) before experiments to prevent their body movements in all imaging sessions. During imaging, slow drifts of the FOV were manually corrected approximately every 40-60 trials based on a reference image. The hair of the mice was shaved to expose their rostral back skin to ensure the effectiveness of the somatosensory stimulation with air puff or heat stimuli.

For opto-itch stimulation, the illumination of the spinal implanted LED was controlled by an Arduino board, which was programmed to also trigger data acquisition of the two-photon imaging system. For each trial, imaging frames during a 2 s baseline period were collected before LED illumination (2 s), and imaging frames during the 11 s poststimulation period were also collected. For the varying intensity session, 120 trials consisting of 5 different intensities with blank control trials were sampled in a randomized manner. In the low intensity or the mCherry control block, 40 trials with a blank control were sampled. The interstimulus interval of the optogenetic stimulation of spinal GRPR$^+$ neurons was set to 20 s.

For the air puff stimuli, air was delivered through a rubber hose connected to a nitrogen cylinder, and the hose tip was pointed at the rostral back skin at a distance of ~1 cm. The delivery of the air puff was gated by an electromagnetic valve controlled by the Arduino board. The weak, medium, and strong air pressures were ~57, ~114, and ~228 kPa, respectively, based on the readings of the cylinder valve. Interstimulus interval of the air puff stimuli was set to 20 s.

For heat stimuli, the tip of a 976 nm infrared laser emitter (Shanghai Laser & Optics Century) was placed ~1.5 cm away from the rostral back skin, and the subcutaneous temperature under different laser powers was measured with a thermometer probe before imaging (Fig. 1). During imaging, delivery of the laser and the different output powers were controlled by the Arduino board. Weak, medium, and strong heat stimuli were delivered with ~0.3, ~0.8, and ~1.2 W lasers, respectively. The interstimulus interval of the heat stimuli was increased to 60 s to prevent skin damage after repeated laser exposure.

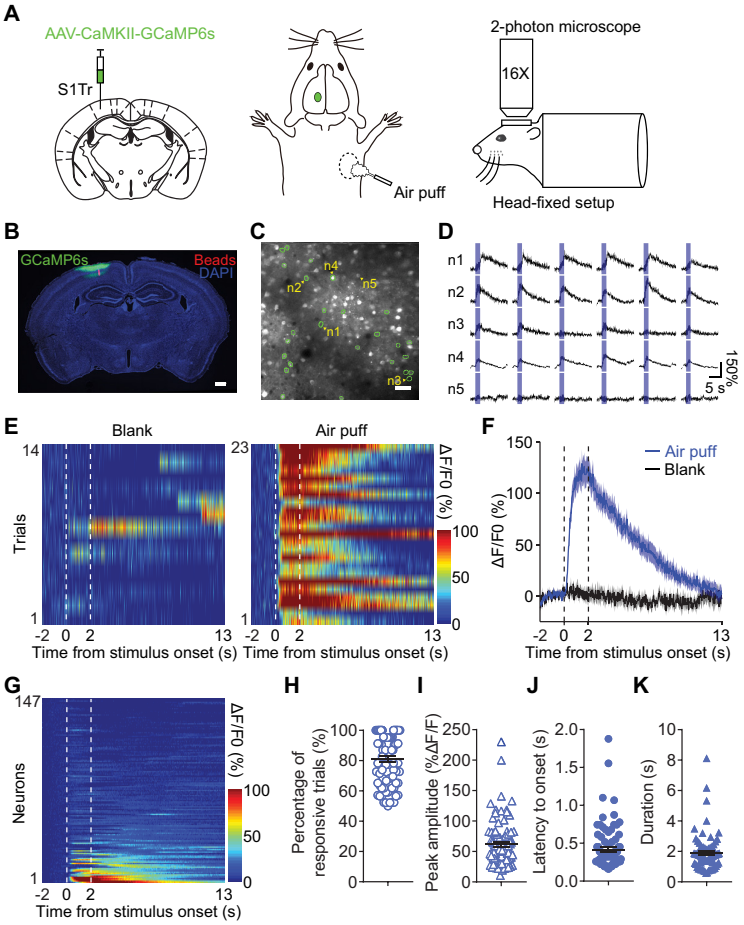

Figure 2. *In vivo* two-photon calcium imaging of S1Tr neurons in response to mechanical stimuli applied to the skin. ***A***, Schematic illustrating AAV-CaMKII-GCaMP6s injection and two-photon imaging of S1Tr in head-fixed mice with mechanical stimuli (~114 KPa air puff). ***B***, Expression of GCaMP6s in S1Tr. The red beads were injected in the middle of the imaging field after the imaging experiment to verify the location of the FOV. Scale bar, 500 μm. ***C***, Image of one example FOV in response to air puff stimuli. Green circles represent neurons that showed significantly activated responses. Scale bar, 50 μm. ***D***, Calcium traces of 5 representative S1Tr pyramidal neurons from ***C*** in response to air puff stimuli in individual trials. Blue shading represents air puff presentation period (2 s). ***E***, Heat maps of the calcium activity of one neuron (n2 in ***D***) responding to air puff stimuli or blank controls. ***F***, Averaged calcium traces of the neurons in ***E*** to air puff stimuli. Shading represents the SEM. Vertical dashed lines indicate the onset and offset of air puff stimuli. ***G***, Heat map of neurons ($n = 147$) from the FOV in ***C*** during the presentation of air puff stimuli. Neurons were rank-ordered by their averaged response magnitude after air puff onset. ***H-K***, Percentage of responsive trials (***H***), peak amplitude (***I***), latency to response onset (***J***), and response duration (***K***) from all defined responsive S1Tr neurons ($n = 85$) responding to air puff stimuli. Error bars indicate SEM.

In sessions with stimuli of different submodalities, 5 Hz 20 mW opto-itch stimulation, ~114 KPa air puff stimuli, and 1.2 W infrared laser-induced heat stimuli were randomly applied with a blank control, for a total of 70 trials. In sessions with stimuli of different submodalities at varying intensities, a total of 170 trials were performed with three different intensities for each stimulus with a blank control.

After finishing the imaging experiments, the location of the imaging field in each mouse was verified via a second injection of red beads in the imaging field. The chronic window was carefully drilled and removed to expose the cortex, and ~100 nl red beads were slowly injected at the center of the imaging field based on vascular landmarks imaged under the two-photon microscope. The injection pipette was withdrawn 5 min after the injection, and mice were then perfused for histology experiments.

Imaging data analysis. Lateral drifts in two-photon images were corrected by an ImageJ plug-in stabilizer (K. Li). Images with excessive drifts were excluded from further analysis. All remaining processing and analysis were performed by custom-written MATLAB codes. ROIs corresponding to visually identifiable somas were then manually outlined.

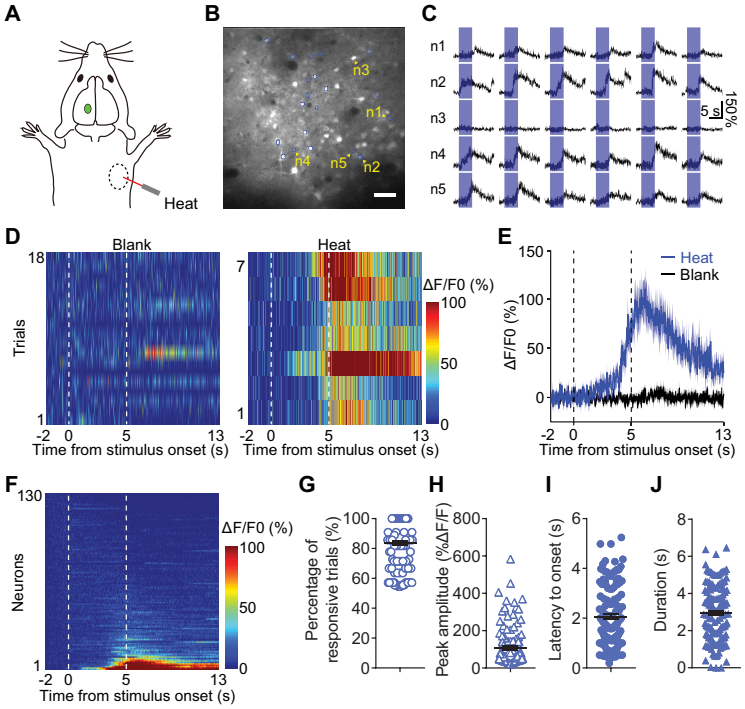

Figure 3. *In vivo* two-photon calcium imaging of S1Tr neurons in response to heat stimuli applied to the skin. ***A***, Schematic illustrating the delivery of infrared laser (~1.2 W)-based heat stimuli to the same somatic region as that air puff stimuli were delivered. ***B***, Image of one example FOV to heat stimuli. Blue circles represent neurons that showed significantly activated responses. Scale bar, 50 μm. ***C***, Calcium traces of 5 representative S1Tr pyramidal neurons from ***B*** in response to heat stimuli in individual trials. Blue shading represents heat presentation period (5 s). ***D***, Heat maps of the calcium activity of one neuron responding to heat stimuli or blank controls. ***E***, Averaged calcium traces of the neuron in ***D*** in response to heat stimuli. Shading represents the SEM. Vertical dashed lines indicate the onset and offset of heat stimuli. ***F***, Heat map of neurons ($n = 130$) from the FOV in ***B*** during the presentation of heat stimuli. Neurons were rank-ordered by their averaged response magnitude after heat stimulus onset. ***G-J***, Percentage of responsive trials (***G***), peak amplitude (***H***), latency to response onset (***I***), and response duration (***J***) from all defined responsive S1Tr neurons ($n = 135$) responding to heat stimuli. Error bars indicate SEM.

The fluorescence of each cell body was measured by averaging the pixels within the ROI, with a correction for neuropil contamination, as previously stated (Chen et al., 2013b). Briefly, the fluorescence of a soma was estimated as $F_{cell\_true}(t) = F_{cell\_measured}(t) - 0.7 \times F_{neuropil}(t)$. The neuropil signal $F_{neuropil}(t)$ surrounding each soma was measured by averaging the signal of all pixels within a 10-pixel radius from the cell center (excluding all selected cells).

For imaging sessions with opto-itch, air puff, or heat stimuli, *F0* was determined by the average of the 2 s period before stimulus onset, and the SD of the baseline was calculated. Neurons were categorized as responsive when the mean $\Delta F/F0$ after stimulus onset (0-4 s for opto-itch and air puff stimuli, 2-7 s for heat stimuli in the 15 s trial) was $>1 \times$ SD higher than baseline in at least 50% of the individual trials. Also, the mean ΔF/F0 after stimulus onset was $>2 \times$ SD higher than the baseline averaged from all trials of the same stimulus. The response onset was defined as the beginning of the first 10 successive sample points $>2 \times$ SD of baseline activity after stimulus onset. The peak was determined as the highest sample point after stimulus onset. The duration of a stimulus-evoked response was determined as the time from the response onset to the peak for a given responsive neuron.

Peak activity averaged from 500 ms (~17 frames) was used for the decoding analysis. For population decoding analysis, we used a support vector machine with a linear kernel (Horikawa et al., 2013). Simultaneously, imaged calcium signals were arranged into an $M \times N$ matrix, where M is the number of trials and N is the number of neurons. Each element in the matrix is the $\Delta F/F0$ of a particular neuron at a given duration in a trial. Eighty percent of trials were randomly selected as the training set, and the remaining 20% trials were used as the test set to evaluate classification accuracy for a population of neurons that was imaged simultaneously. This process was repeated 1000 times, and the averaged testing dataset accuracy was used as the population classification accuracy. A shuffled dataset was generated by shuffling the labels of all trials, and the same procedure was performed. To minimize any dependencies on the intensity of neuron activity aroused by different stimuli, $\Delta F/F0$ was normalized for each stimulus type so the maximum $\Delta F/F0$ for each stimulus type equaled 1. The same process of population decoding was performed to test the decoding accuracy among different trial types. For the training set, the number of trials with different labels was balanced.

Statistical analysis. The sample size of each experiment is provided in Results and figure legends. The data are presented as mean ± SEM. All statistical analyses were performed using GraphPad Prism 6 and MATLAB 2014a. Statistical significance was set at $p < 0.05$, and p values < 0.001 are reported as $p < 0.001$. The Friedman test with Dunn's multiple comparisons was used to assess the differences in the trial-by-trial reliability or peak response amplitude of S1 responses to different opto-itch intensities across groups or to different stimuli across groups. The Mann–Whitney test was used to assess the differences between the S1Tr and S1BF in the percentage of neurons that responded to different stimuli. The Kolmogorov–Smirnov test was used to assess the differences in the cumulative distribution of the peak amplitude between the neurons in the opto-itch and control groups or the differences in the cumulative distribution of interneuronal distances between groups.

Results

A proportion of S1Tr pyramidal neurons are activated by mechanical or thermal stimuli

To examine how somatosensory information of different submodalities is processed in S1 at the single-neuron level, we used *in vivo* two-photon calcium imaging to monitor the activity of S1 neurons in head-fixed mice under quiet awake conditions (Petreanu et al., 2012) while delivering somatosensory stimuli to the same somatic region (Fig. 2*A*). We expressed GCaMP6s (Chen et al., 2013b) in the pyramidal neurons of S1Tr, the S1 subregion corresponding to the trunk area (Fig. 2*B*). In response to mechanical stimuli (air puff), ~14.9% (248 of 1665) of layer 2/3 S1Tr pyramidal neurons were reliably activated (Fig. 2*C–H*), and the response profile reflected the fast kinetics of the mechanical stimuli (Fig. 2*I–K*). When delivering thermal stimuli (heat) using an infrared laser emitter (Fig. 3*A*), we observed a comparable proportion (12.3%, 204 of 1665) of activated S1Tr neurons (Fig. 3*B–F*). S1Tr neurons that were responsive to thermal stimuli exhibited high trial-by-trial reliability (Fig. 3*G*). However, the response kinetics, including the peak amplitude, latency to response onset, and duration of the response to the thermal stimuli, were rather different from those to the air puff stimuli (Fig. 3*H–J*), likely reflecting the differential kinetics of these two somatosensory stimuli. However, the fraction of neurons

responsive to these stimuli was smaller than that in some previous studies measuring S1 neuronal responses to cooling or tactile stimuli (Milenkovic et al., 2014). We reasoned that this discrepancy might have been caused by the variable sensitivity of different body parts, as we applied the stimuli to the animals' trunk skin, while other studies stimulated the animals' whiskers or paws (Chen et al., 2013a; Prsa et al., 2019). Thus, our population imaging results demonstrated sparse coding of mechanical and thermal sensation in the primary somatosensory cortex, consistent with that observed in previous studies (Jadhav et al., 2009; Barth and Poulet, 2012).

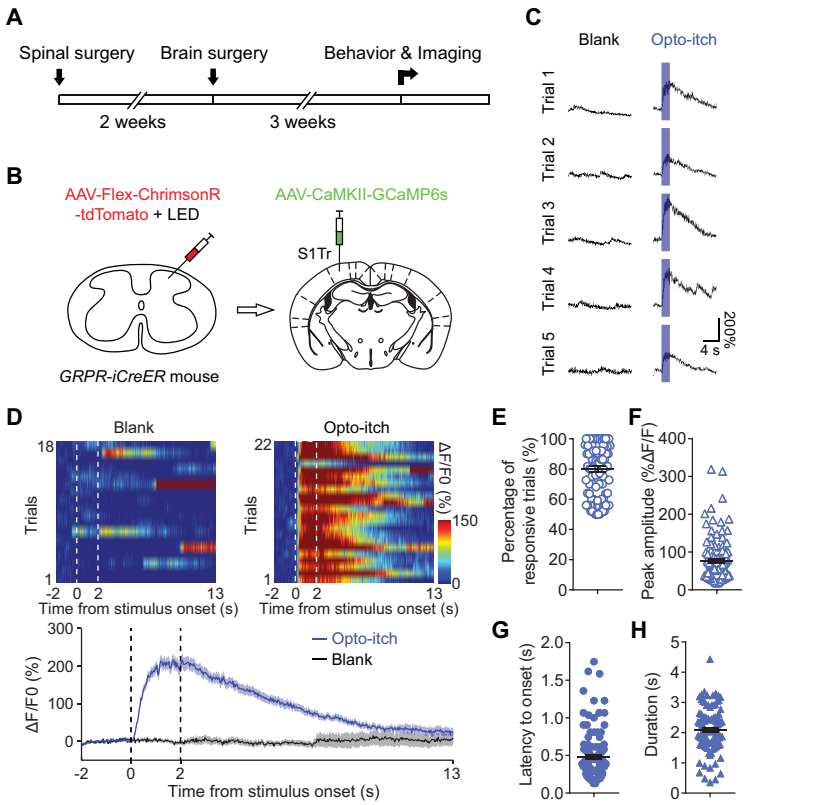

Figure 4. S1Tr neurons were reliably activated by opto-itch stimuli. ***A***, Experimental timeline for calcium imaging of S1Tr in response to opto-itch stimuli. ***B***, Schematic of AAV-Flex-ChrimsonR-tdTomato injection and red LED implantation in the cervical spinal cord, followed by AAV-CaMKII-GCaMP6s injection and chronic window implantation in the contralateral S1Tr in *GRPR-iCreER* mice. ***C***, Calcium traces of one example neuron responding to opto-itch stimuli (5 Hz, 20 mW) in individual trials. Blue shading represents opto-itch stimulation period (2 s). ***D***, Top, Heat maps of the calcium activity of the example neuron in ***C*** responding to opto-itch stimuli or blank controls. Bottom, Averaged calcium traces of this neuron in response to opto-itch stimuli. Vertical dashed lines indicate the onset and offset of opto-itch stimuli. ***E–H***, Percentage of responsive trials (***E***), peak amplitude (***F***), latency to response onset (***G***), and response duration (***H***) from all defined responsive S1Tr neurons ($n = 110$) responding to opto-itch stimuli. Error bars indicate SEM.

Itch is encoded by both individual S1Tr neurons and populations of S1Tr neurons

The itch sensation represents another important submodality of somatosensation, for which the cortical representation is largely unknown. The difficulty in examining itch-evoked cortical responses at high temporal resolution is that the timing of itch sensation evoked by pruritogens cannot be precisely determined. We thus developed an opto-itch model by expressing ChrimsonR in spinal itch-selective GRPR$^+$ neurons (Sun et al., 2009; Klapoetke et al., 2014; Liu et al., 2020) and used optogenetics to activate these neurons to evoke itch sensations with precisely controlled timing and intensity. To examine the responses of S1Tr neurons to optogenetically induced itch sensations, we performed two-photon imaging of the S1Tr region while photostimulating spinal GRPR$^+$ neurons (Fig. 4*A*,*B*). We found that optogenetic stimulation of spinal GRPR$^+$ neurons evoked strong activation of S1Tr neurons with high trial-to-trial reliability (Fig. 4*C–H*), and individual neurons showed increased response amplitude in a graded fashion when the opto-itch intensity was increased (Fig. 5*A*,*B*). At the population level, ~12.6% (76 of 603) of S1Tr pyramidal neurons exhibited significant responses to opto-itch stimuli at lower intensity (5 Hz, 5 mW). Stronger opto-itch stimuli recruited more S1Tr neurons, and a group of neurons (>1/4 of all responsive neurons) was activated at all intensities (Fig. 5*C–E*). With the increase in opto-itch stimulus intensity, the trial-by-trial reliability and peak amplitude increased, while the latency to response onset decreased ($p < 0.001$, Friedman test with Dunn's multiple comparisons; Fig. 5*F–H*). This latency mirrors the latency of the scratching behavior induced by photostimulation of spinal GRPR$^+$ neurons (Fig. 5*H*).

In contrast, subliminal photostimulation of spinal GRPR$^+$ neurons (5 Hz, 1 mW), which could not evoke scratching behavior, elicited no significant responses in S1Tr neurons ($p < 0.001$, Kolmogorov–Smirnov test; Fig. 5*I–L*). To exclude the possibility that the heating of the spinal cord elicited by red-light illumination activated S1Tr neurons nonspecifically, we expressed mCherry in spinal GRPR$^+$ neurons of one batch of mice and found that red-light illumination indeed did not evoke significant S1Tr responses ($p < 0.001$, Kolmogorov–Smirnov test; Fig. 5*M–P*). These data suggested that the activation of S1Tr neurons was dependent on the pruritic input evoked by sufficient optogenetic activation of spinal GRPR$^+$ neurons. Together, our data supported the proposition that the primary somatosensory cortex encodes the temporal and intensity aspects of itch sensation (LaMotte et al., 2014).

Topographic representation of somatosensation in S1

To examine whether cortical responses evoked by mechanical, thermal, and pruritic stimuli exhibit topographic organization in S1, we performed two-photon calcium imaging of the S1BF, the vibrissal somatosensory cortex (Fig. 6*A*,*B*); we also delivered the same somatosensory stimuli in the same area as that in the S1Tr experiments. We found that very few S1BF pyramidal neurons were activated by these somatosensory stimuli (Fig. 6*C–E*). The proportion of imaged S1BF neurons that responded to heat and opto-itch stimuli was significantly smaller than that of the S1Tr neuronal population (opto-itch: $p = 0.008$, heat: $p = 0.016$, Mann–Whitney test; Fig. 6*F*,*H*). The proportion of mechanoresponsive S1BF neurons showed a prominent decreasing trend compared with that of S1Tr neurons, although no significant difference was reached under this condition ($p = 0.095$, Mann–

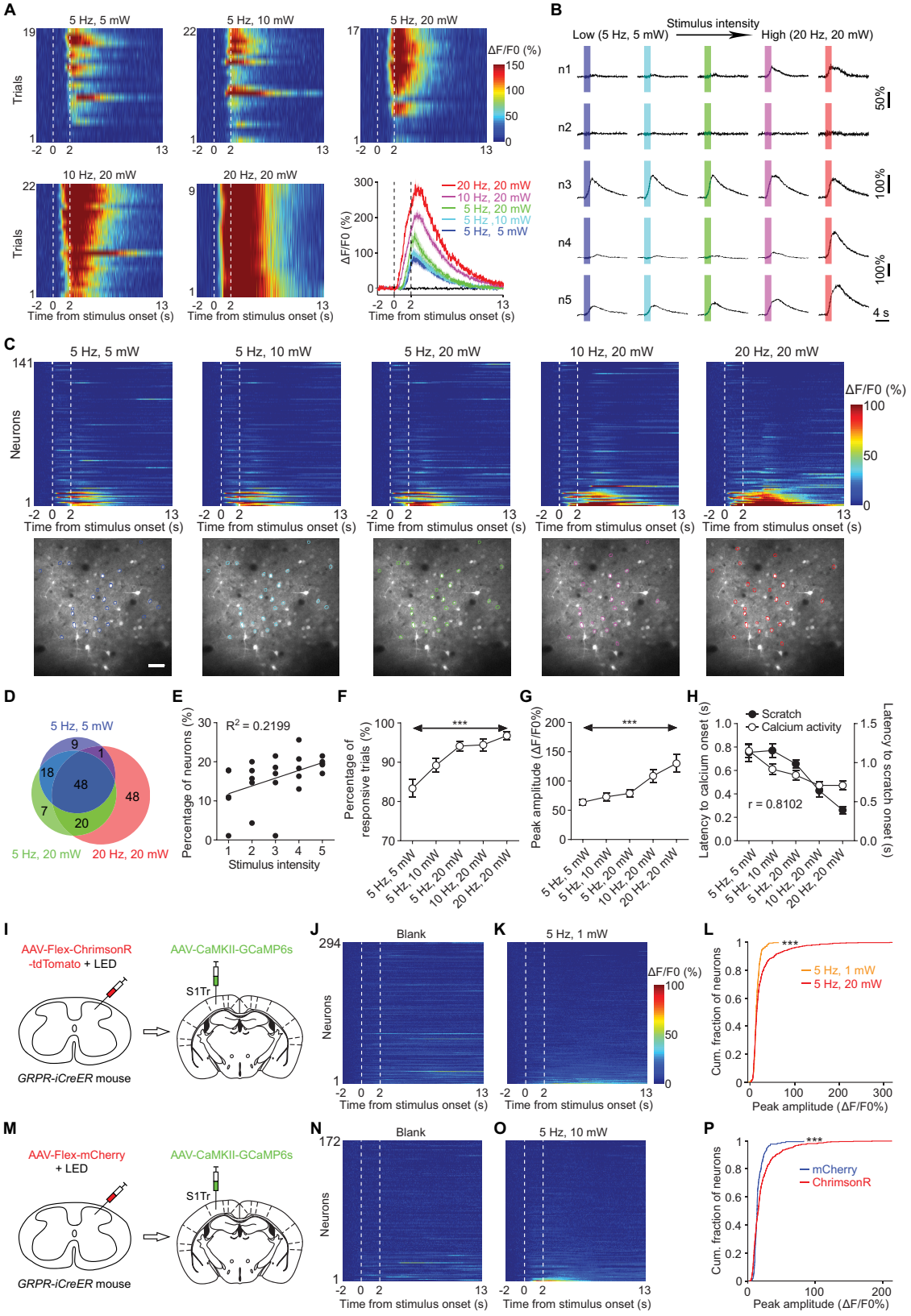

Figure 5. Coding of itch in S1Tr. ***A***, Heat maps of the calcium activity of one example neuron in response to opto-itch stimuli at different intensities. Bottom right, Averaged calcium response of this neuron. Shading area represents the SEM. Vertical dashed lines indicate the onset and offset of opto-itch stimuli. ***B***, Averaged calcium traces of 5 neurons in response to opto-itch stimuli at different intensities. Neuron n2 is an example neuron that does not show a positive response to opto-itch stimuli. Shading represents opto-itch stimulation period. Colors correspond to those of the traces in ***A***. ***C***, Population dynamics of S1Tr pyramidal neurons to opto-itch stimuli. Top, Heat maps of neurons ($n = 141$) from one example FOV in response to opto-itch stimuli. Neurons were rank-ordered by their averaged response magnitude after opto-itch onset in 20 Hz, 20 mW trials. Each row represents responses from the same neuron at different intensities. Bottom, Images of the same FOV at different intensities. Colored circles represent neurons that showed significantly activated responses. Scale bar, 50 μm. ***D***, Number of responsive neurons (out of 603 neurons from 5 mice) in low-, medium-, and high-intensity trials. ***E***, Percentage of responsive neurons in response to opto-itch stimuli at different intensities. Each black dot represents the percentage of responsive neurons in 1 mouse at the

Whitney test; Fig. 6*G*). These data suggested that sensory-evoked responses in S1 exhibited explicit regional specificity, supporting the somatotopic organization in S1 for processing different somatosensory information.

Representation of different somatosensations in S1Tr

It has been proposed that multiple submodalities of somatosensation could be represented by the same area within the primary somatosensory cortex based on somatotopic organization (Penfield and Boldrey, 1937; Woolsey and Van der Loos, 1970; Kaas et al., 1979), but the coding mechanism is still not well understood. To explore how the primary somatosensory cortex encodes different somatosensory submodalities, we imaged the same population of S1Tr pyramidal neurons with the application of different submodalities of somatosensory stimuli (i.e., mechanical, thermal, and pruritic stimuli). We found that a significant proportion of S1Tr neurons were activated by all three types of stimuli, whereas others responded to one or two types of stimuli (Fig. 7*A–F*). Moreover, a comparable proportion of S1Tr neurons were activated by these different stimuli (Fig. 7*G*,*H*). Within the imaged neuronal population, >13.1% (218 of 1665) of the recorded S1Tr pyramidal neurons were activated by two or three different submodalities of stimuli, and ~12.3% (205 of 1665) of recorded neurons were activated by only one somatosensory submodality (Fig. 7*I*).

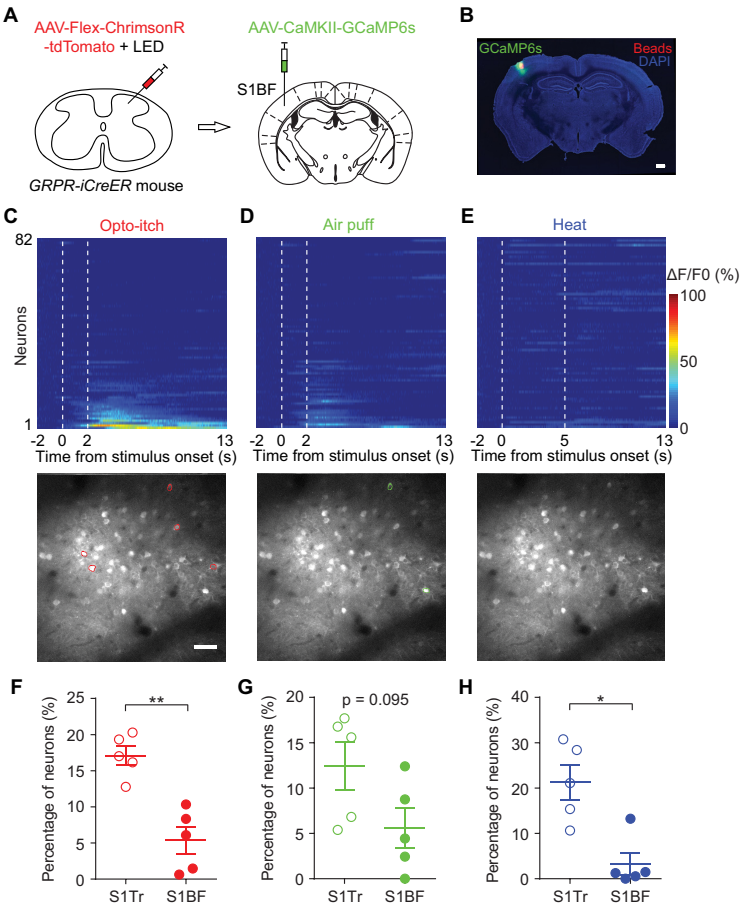

Figure 6. Topographic specificity of sensory-evoked responses in S1. ***A***, Schematic of AAV-Flex-ChrimsonR-tdTomato injection in the cervical spinal cord, followed by AAV-CaMKII-GCaMP6s injection in the contralateral S1BF of *GRPR-iCreER* mice. ***B***, Expression of GCaMP6s in S1BF. The red beads were injected in the center of the imaging field after the imaging experiment to verify the location of the FOV. Scale bar, 500 μm. ***C-E***, Population dynamics of S1BF pyramidal neurons in response to different somatosensory stimuli. Top, Heat maps of neurons ($n = 82$) from one example FOV during the presentation of different stimuli. Neurons were rank-ordered by their averaged response magnitude to opto-itch stimuli. Each row represents responses from the same neuron. Vertical dashed lines indicate the onset and offset of stimuli. Bottom, Images of the same FOV to different stimuli. Colored circles represent neurons that showed significantly activated responses. Scale bar, 50 μm. ***F-H***, Comparison of the percentage of responsive neurons responding to opto-itch (***F***), air puff (***G***), or heat stimuli (***H***) in S1Tr and S1BF ($n = 5$ mice). $^*p < 0.05$; $^{**}p < 0.01$; Mann–Whitney test. Error bars indicate SEM.

Given the substantial overlap of S1Tr neurons responding to different stimuli, we asked whether these imaged neurons encoded sufficient information to distinguish different somatosensory submodalities. We thus performed population decoding analysis. Since the response kinetics of S1Tr neurons to different stimuli were rather diverse (trial-by-trial reliability: $p = 0.013$, peak amplitude: $p < 0.001$, Friedman test with Dunn's multiple comparisons; Figs. 2*H–K*, 3*G–J*, 4*E–H*, and 7*J*,*K*), these features could potentially be used by the decoder to easily distinguish different somatosensory stimuli. To pre-exclude this potential confound, we performed population decoding analysis using the peak amplitude of responses in individual trials with different stimuli. We quantified how well the S1Tr population decoded different submodalities of somatosensory information using a support vector machine with a linear kernel across different stimulus trials. The classifier attempted to decode the stimulus types from the peak activity of all simultaneously imaged neurons (see Materials and Methods). We found that the classifier could indeed distinguish different types of stimuli with high accuracy (Fig. 7*L*). The overall response amplitudes of S1Tr

←

corresponding intensity. Solid line is a linear regression fit to the black dots. ***F***, ***G***, Trial-by-trial reliability (***F***) and peak amplitude (***G***) of the same responsive S1Tr neurons ($n = 45$) responding to different opto-itch intensities. Friedman test with Dunn's multiple comparisons. ***H***, Response latency to S1Tr activation (left *y* axis) and the behavioral latency to scratch (right *y* axis) in response to opto-itch stimuli at different intensities. The two curves showed strong correlation. ***I***, Schematic of AAV-Flex-ChrimsonR-tdTomato injection in the cervical spinal cord, followed by AAV-CaMKII-GCaMP6s injection in the contralateral S1Tr of *GRPR-iCreER* mice. ***J***, ***K***, Heat maps of neurons ($n = 294$ neurons) in response to subliminal opto-itch stimuli (5 Hz, 1 mW) or blank controls. Neurons were rank-ordered by their averaged activity magnitude after light onset in 5 Hz, 1 mW trials. Each row represents responses from the same neuron. ***L***, Cumulative distribution of averaged peak amplitude after light onset for neurons to subliminal or supraliminal opto-itch stimuli (294 neurons in 5 Hz, 1 mW, 649 neurons in 5 Hz, 20 mW trials). Kolmogorov–Smirnov test. Cum., Cumulative. ***M***, Schematic of AAV-Flex-mCherry injection in the cervical spinal cord, followed by AAV-CaMKII-GCaMP6s injection in the contralateral S1Tr of *GRPR-iCreER* mice. ***N***, ***O***, Heat maps of neurons in response to LED illumination in the spinal cord of *GRPR-iCreER* mice injected with AAV-Flex-mCherry. Neurons were rank-ordered by their averaged activity magnitude after light onset in 5 Hz, 10 mW trials. Each row represents responses from the same neuron. ***P***, Cumulative distribution of averaged peak amplitude of neurons in response to LED illumination after light onset (5 Hz, 10 mW) in mice injected with ChrimsonR ($n = 603$ neurons) or mCherry ($n = 172$ neurons). $^{***}p < 0.001$ (Kolmogorov–Smirnov test). Error bars indicate SEM.

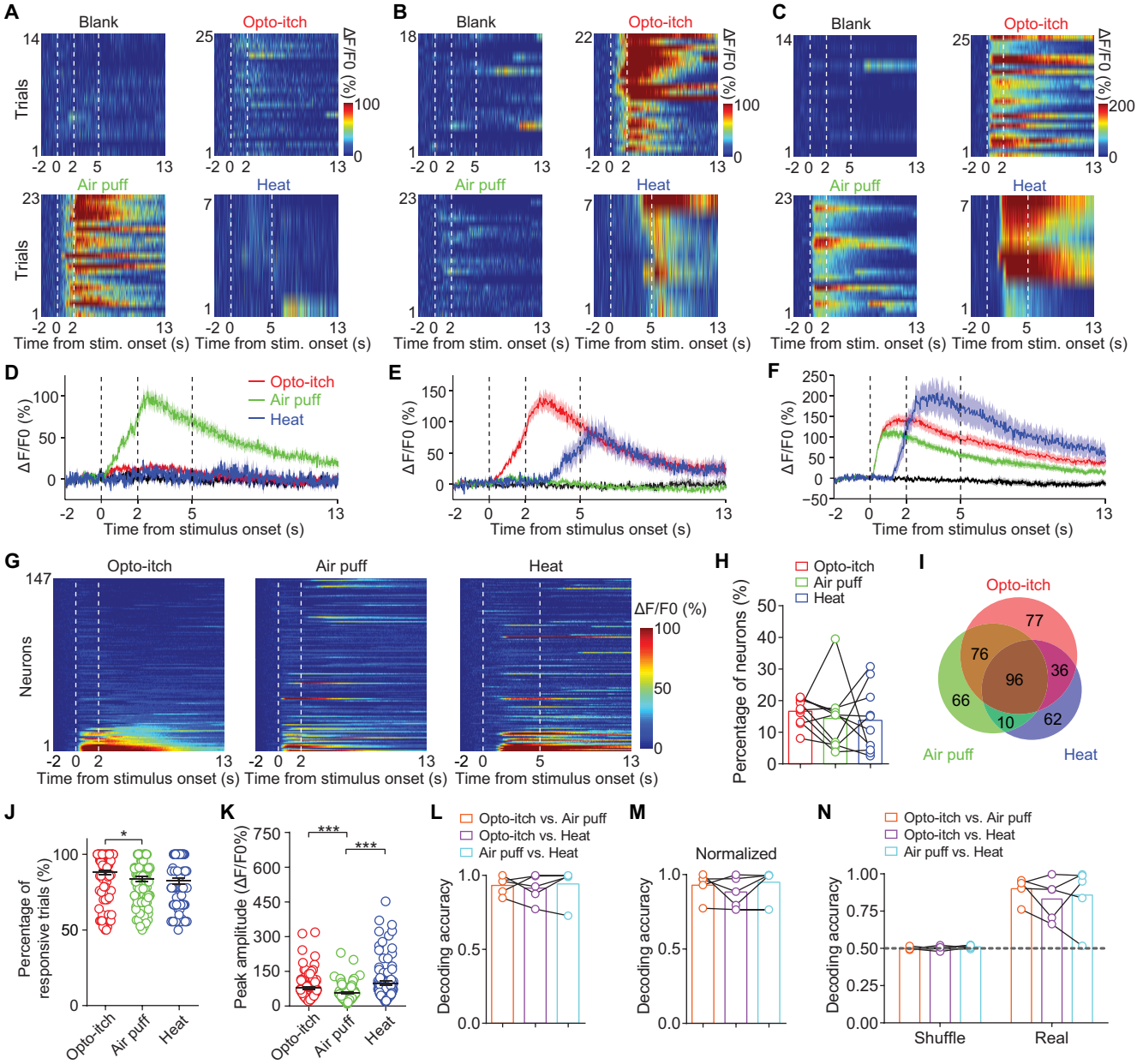

Figure 7. Representation of different somatosensations in S1Tr. ***A-C***, Heat maps of the calcium activity of three example neurons in response to opto-itch (5 Hz, 20 mW), air puff, and heat stimuli. Stim., Stimulus. ***D-F***, Averaged calcium responses of neurons in ***A-C*** to different stimuli. Shading represents the SEM. Vertical dashed lines indicate the onset and offset of different stimuli. ***G***, Heat maps of neurons ($n = 147$) from one example FOV during the presentation of different stimuli. Neurons were rank-ordered by their response magnitude to opto-itch stimuli. Each row represents responses from the same neuron to different stimuli. ***H***, Percentage of S1Tr neurons responsive to opto-itch, air puff, and heat stimuli (10 FOVs from 10 mice). Connected colored dots represent the value from the same mouse to different stimuli. ***I***, Number of responsive S1Tr neurons (out of 1665 neurons from 10 mice) in response to different stimuli. ***J***, ***K***, Trial-by-trial reliability (***J***) and peak amplitude (***K***) of the same S1Tr responsive neurons ($n = 96$) responding to different stimuli. Friedman test with Dunn's multiple comparisons. ***L***, ***M***, Decoding accuracy of different stimuli with one fixed intensity from all imaged S1Tr neurons before (***L***) and after normalization (***M***) of the response amplitude ($n = 5$ mice). ***N***, Decoding accuracy of different stimuli with one fixed intensity from S1Tr neurons responsive to all three different types of stimuli ($n = 5$ mice). Connected colored dots represent the value from the same mouse under different conditions. $^{*}p < 0.05$. $^{***}p < 0.001$. Error bars indicate SEM.

neurons were different for the three types of stimuli ($p < 0.001$, Friedman test with Dunn's multiple comparisons; Fig. 7*K*), which could potentially be used by the classification decoder. To examine this possibility, we normalized the response amplitude of all neurons within each stimulus type and used the normalized activity for the decoding analysis. Different types of stimuli could still be decoded with high accuracy after normalization (Fig. 7*M*), suggesting that the decoding of different stimuli by S1Tr neurons was not solely dependent on the difference in response amplitudes. Given that ~5.8% (96 of 1665) of S1Tr neurons responded to all three stimuli, we investigated whether these neurons alone encode a sufficient amount of information to distinguish different somatosensory submodalities. We thus performed decoding analysis using this small population of neurons and found that the decoding accuracy was still above chance level (Fig. 7*N*), although the absolute accuracy was lower than that using all imaged S1Tr neurons (Fig. 7*L*,*M*). Thus, S1Tr neurons could encode different somatosensations with a population coding scheme.

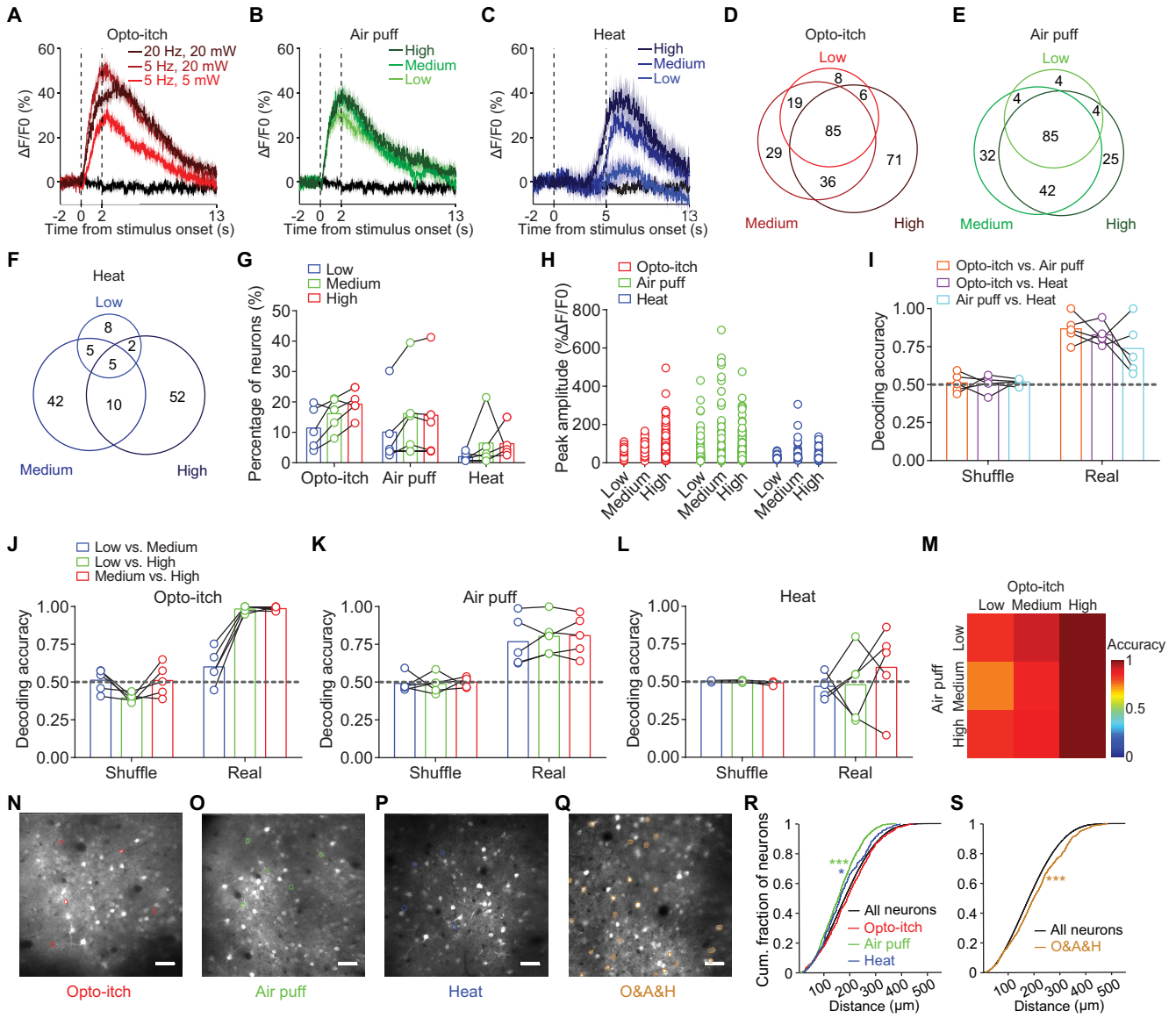

Figure 8. Decoding of different somatosensory submodalities in S1Tr. ***A-C***, Averaged calcium responses of one example neuron responding to opto-itch (***A***), air puff (***B***), and heat stimuli (***C***) at varying intensities. Shading represents the SEM. Vertical dashed lines indicate the onset and offset of stimuli. ***D-F***, Number of responsive S1Tr neurons (out of 1016 neurons from 5 mice) in low-, medium-, and high-intensity opto-itch (***D***), air puff (***E***), or heat (***F***) trials. ***G***, Percentage of responsive S1Tr neurons in response to stimuli at different intensities ($n = 5$ mice). Connected colored dots represent the value from the same mouse at different intensities. ***H***, Peak amplitude of responsive S1Tr neurons to stimuli at different intensities. ***I***, Decoding accuracy of different stimuli with mixed intensities from all imaged S1Tr neurons ($n = 5$ mice). Connected colored dots represent the value from the same mouse under different conditions. ***J-L***, Decoding accuracy of different intensities of opto-itch (***J***), air puff (***K***), or heat (***L***) stimuli from all imaged S1Tr neurons ($n = 5$ mice). Connected colored dots represent the value from the same mouse under different conditions. ***M***, Matrix of decoding accuracy (averaged from 5 mice) of opto-itch versus air puff stimuli at different intensities from all imaged S1Tr neurons. ***N-Q***, Images of example FOVs to different stimuli. Colored circles represent neurons that were selectively activated by opto-itch (***N***), air puff (***O***), or heat (***P***) stimuli, or significantly activated by all three different types of stimuli (***Q***). O&A&H, Opto-itch & Air puff & Heat. Scale bar, 50 μm. ***R***, Cumulative distribution of pairwise distances among neurons selectively activated by air puff, heat, or opto-itch stimuli as well as all S1Tr neurons (1103 air puff, 281 heat, 347 opto-itch, and 148,750 all-neuron pairs from 10 mice). Cum., Cumulative. ***S***, Cumulative distribution of pairwise distances among neurons simultaneously activated by all three types of stimuli as well as all S1Tr neurons (777 responsive neurons and 148,750 all-neuron pairs from 10 mice). *$p < 0.05$; ***$p < 0.001$; Kolmogorov–Smirnov test. Error bars indicate SEM.

To further demonstrate that the decoding ability of S1Tr neurons is not simply dependent on the overall difference in the response amplitude, we imaged the same population of S1Tr neurons while delivering three types of stimuli with different intensities. The percentage of responsive S1Tr neurons and the peak amplitude of individual neurons showed an increasing trend with increasing stimulus intensity (Fig. 8*A–H*). We pooled trials with different stimulus intensities and performed decoding analysis using the peak activity of all recorded S1Tr neurons. We found that the population decoder could still distinguish different stimulus types with decoding accuracy comparable to that noted when using data of a single stimulus intensity (Figs. 7*L*,*M* and 8*I*). Next, we grouped trials from different stimuli based on varying levels of stimulus intensity (low, medium, and high) and performed decoding analysis between each pair of possible intensities of one given somatosensory stimulus, as well as between two stimulus types with different combinations of intensity levels. We found that the S1Tr neuronal population could reliably distinguish these stimulus types regardless of the stimulus intensity (Fig. 8*J–M*), further confirming that the decoding ability of S1Tr neurons is not simply dependent on the difference in response amplitudes.

Together, these data suggested that layer 2/3 pyramidal neurons in S1Tr encode sufficient information to differentiate multiple submodalities of somatosensory stimuli.

Next, we examined whether S1Tr neurons with similar submodality preferences exhibited spatial clustering. Among S1Tr neurons that were selectively activated by mechanical or thermal stimuli, pairwise distances between neurons within either group were smaller than distances among all neurons in the imaging field (air puff: $p < 0.001$, heat: $p = 0.014$, Kolmogorov–Smirnov test; Fig. 8*O*,*P*,*R*). Interestingly, unlike S1Tr neurons that prefer mechanical or thermal stimuli, the distances among neurons selectively activated by pruritic stimuli were comparable to the distances among all recorded neurons ($p = 0.378$, Kolmogorov–Smirnov test; Fig. 8*N*,*R*). It is possible that optogenetically activated $GRPR^+$ neurons covered more spinal cord segments than mechanical or thermal stimuli that were applied peripherally, which in turn recruited more widely distributed S1Tr neurons in the imaging field. Interestingly, for S1Tr neurons that showed reliable responses to all three different types of stimuli, the pairwise distances were even slightly larger than the distances among all recorded neurons ($p < 0.001$, Kolmogorov–Smirnov test; Fig. 8*Q*,*S*). Although these neurons were activated by different stimuli without submodal specificity, the activation pattern of the same population was variable (trial-by-trial reliability: $p = 0.013$, peak amplitude: $p < 0.001$, Friedman test with Dunn's multiple comparisons; Fig. 7*J*,*K*). Thus, S1Tr neurons with a response preference for mechanical or thermal stimuli exhibited spatial clustering.

Discussion

In this study, we revealed the representation of multiple submodalities of somatosensation in S1 at the cellular level, which extended the findings of previous fMRI and electrophysiological studies showing that somatosensory stimuli of different submodalities could activate the same subregion or individual neurons in S1 (Pei et al., 2009; Mancini et al., 2012; Milenkovic et al., 2014; Khasabov et al., 2020). Our data indicate that there are both unimodal and multimodal neurons in S1, especially when considering the responses when mechanical and thermal stimuli were applied in the same somatic region. These results are consistent with previous findings that both the segregation and convergence of S1 responses elicited by stimuli with different submodalities were detected (Sur et al., 1981; Ploner et al., 2000; Friedman et al., 2004; Pei et al., 2009; Milenkovic et al., 2014). In addition, the multiplexed response profile of S1 coincided with the observation that spinal projection neurons relaying somatosensory information to the brain exhibit a similar response pattern to multiple somatosensory stimuli (Davidson et al., 2007; Davidson and Giesler, 2010). One caveat of this study is that opto-itch stimuli were delivered by activation of spinal neurons; thus, the area in S1 activated by opto-itch stimuli is likely larger than that activated by mechanical or thermal stimuli applied in the skin. In future studies, it would be nice to specifically activate itch-selective sensory fibers within one dermatome to produce a more localized pruritic stimulus, thus enabling a fairer direct comparison between S1 responses evoked by pruritic versus other somatosensory stimuli.

Our study revealed the graded coding scheme of itch sensation in S1 at the single-neuron level and the population level. Also, itch intensity was reflected in the response magnitude of individual neurons, as well as in the size of the responsive neuron population. The coding scheme of itch in S1 is similar to the coding strategy of heat in peripheral afferents and the spinal cord (Ran et al., 2016; Wang et al., 2018). Our results are also consistent with previous observations that the intensity of subjective itch intensity was highly correlated with the neuronal activity of S1, as indicated by PET or fMRI (Darsow et al., 2000; Drzezga et al., 2001; Holle et al., 2012). Moreover, the present findings provide a more in-depth perspective for the coding mechanism of itch in the somatosensory cortex at the cellular level.

We examined the topographic representation of different somatosensations in S1 by imaging another S1 subregion, S1BF, as a control, while applying stimuli to the trunk area and verified the somatotopic specificity of sensory-evoked S1 responses (Penfield and Boldrey, 1937; Woolsey and Van der Loos, 1970). We noted that there was still a small fraction of S1BF neurons that exhibited increased activity during sensory stimulation; this activity could be partly attributed to the background activity of S1BF because of active whisking (Crochet et al., 2011; Chen et al., 2013a). In addition, stimuli applied in the rostral back skin or rostral cervical spinal cord might overlap slightly with the caudal receptive field of S1BF. Choosing another S1 subregion or trimming the whiskers before imaging might further reduce this effect.

Our study also demonstrated that the activity of the S1 neuronal population is capable of encoding different somatosensory submodalities, supporting the proposition that perceptual distinction between different somatosensory stimuli can be achieved in primary sensory cortices (Parker and Newsome, 1998; Ma, 2010; LaMotte et al., 2014; Dong and Dong, 2018). Given that different somatosensory submodalities could still be decoded using the subfraction of S1 neurons showing multimodal responses, the population code for sensory differentiation probably lies in a rather finite number of S1 neurons. The population coding mechanism of different somatosensations in S1 was proposed by previous studies but has not yet been thoroughly verified because of the limited sample size of recorded neurons in single-unit electrophysiological experiments (Milenkovic et al., 2014; Khasabov et al., 2020). Our population imaging data compensated for this disadvantage and indeed supported the population coding hypothesis for somatosensation.

It is interesting that some S1 neurons selectively respond to one stimulus while other neurons are multimodal and are capable of distinguishing different stimuli. We speculate that the combination of neurons with different response properties endows S1 with more power to code complex sensations (mechanical itch, thermal pain, etc.), and to better undergo sensory integration by recruiting differential neuron populations. Because of the intrinsically sparse coding property of layer 2/3 S1 neurons (Barth and Poulet, 2012; Petersen and Crochet, 2013; Adesnik and Naka, 2018), the precise level of segregation between different submodalities at the single-neuron level still remains to be determined; thus, population coding provides a potential mechanism to ensure the smooth processing of multimodal sensory information. Together, our findings provide new mechanistic insights into the coding scheme of mechanical, thermal, and itch sensations in the primary somatosensory cortex and extend our knowledge of multimodal somatosensory processing and integration in the cerebral cortex.

References

Adesnik H, Naka A (2018) Cracking the function of layers in the sensory cortex. Neuron 100:1028–1043.

Andrew D, Craig AD (2001) Spinothalamic lamina I neurons selectively sensitive to histamine: a central neural pathway for itch. Nat Neurosci 4:72–77.

Barth AL, Poulet JF (2012) Experimental evidence for sparse firing in the neocortex. Trends Neurosci 35:345–355.
Brown J, Oldenburg IA, Telian GI, Griffin S, Voges M, Jain V, Adesnik H (2021) Spatial integration during active tactile sensation drives orientation perception. Neuron 109:1707–1720.e1707.
Carstens E (1997) Responses of rat spinal dorsal horn neurons to intracutaneous microinjection of histamine, capsaicin, and other irritants. J Neurophysiol 77:2499–2514.
Chen JL, Carta S, Soldado-Magraner J, Schneider BL, Helmchen F (2013a) Behaviour-dependent recruitment of long-range projection neurons in somatosensory cortex. Nature 499:336–340.
Chen TW, Wardill TJ, Sun Y, Pulver SR, Renninger SL, Baohan A, Schreiter ER, Kerr RA, Orger MB, Jayaraman V, Looger LL, Svoboda K, Kim DS (2013b) Ultrasensitive fluorescent proteins for imaging neuronal activity. Nature 499:295–300.
Crochet S, Poulet JF, Kremer Y, Petersen CC (2011) Synaptic mechanisms underlying sparse coding of active touch. Neuron 69:1160–1175.
Darsow U, Drzezga A, Frisch M, Munz F, Weilke F, Bartenstein P, Schwaiger M, Ring J (2000) Processing of histamine-induced itch in the human cerebral cortex: a correlation analysis with dermal reactions. J Invest Dermatol 115:1029–1033.
Davidson S, Giesler GJ (2010) The multiple pathways for itch and their interactions with pain. Trends Neurosci 33:550–558.
Davidson S, Zhang X, Yoon CH, Khasabov SG, Simone DA, Giesler GJ Jr (2007) The itch-producing agents histamine and cowhage activate separate populations of primate spinothalamic tract neurons. J Neurosci 27:10007–10014.
Dong X, Dong X (2018) Peripheral and central mechanisms of itch. Neuron 98:482–494.
Drzezga A, Darsow U, Treede RD, Siebner H, Frisch M, Munz F, Weilke F, Ring J, Schwaiger M, Bartenstein P (2001) Central activation by histamine-induced itch: analogies to pain processing: a correlational analysis of O-15 H_2O positron emission tomography studies. Pain 92:295–305.
Emery EC, Luiz AP, Sikandar S, Magnusdottir R, Dong X, Wood JN (2016) In vivo characterization of distinct modality-specific subsets of somatosensory neurons using GCaMP. Sci Adv 2:e1600990.
Friedman RM, Chen LM, Roe AW (2004) Modality maps within primate somatosensory cortex. Proc Natl Acad Sci USA 101:12724–12729.
Gao ZR, Chen WZ, Liu MZ, Chen XJ, Wan L, Zhang XY, Yuan L, Lin JK, Wang M, Zhou L, Xu XH, Sun YG (2019) Tac1-expressing neurons in the periaqueductal gray facilitate the itch-scratching cycle via descending regulation. Neuron 101:45–59.e49.
Hachisuka J, Baumbauer KM, Omori Y, Snyder LM, Koerber HR, Ross SE (2016) Semi-intact ex vivo approach to investigate spinal somatosensory circuits. eLife 5:e22866.
Han L, Ma C, Liu Q, Weng HJ, Cui Y, Tang Z, Kim Y, Nie H, Qu L, Patel KN, Li Z, McNeil B, He S, Guan Y, Xiao B, Lamotte RH, Dong X (2013) A subpopulation of nociceptors specifically linked to itch. Nat Neurosci 16:174–182.
Holle H, Warne K, Seth AK, Critchley HD, Ward J (2012) Neural basis of contagious itch and why some people are more prone to it. Proc Natl Acad Sci USA 109:19816–19821.
Horikawa T, Tamaki M, Miyawaki Y, Kamitani Y (2013) Neural decoding of visual imagery during sleep. Science 340:639–642.
Ikoma A, Steinhoff M, Stander S, Yosipovitch G, Schmelz M (2006) The neurobiology of itch. Nat Rev Neurosci 7:535–547.
Isett BR, Feasel SH, Lane MA, Feldman DE (2018) Slip-based coding of local shape and texture in mouse S1. Neuron 97:418–433.e415.
Jadhav SP, Wolfe J, Feldman DE (2009) Sparse temporal coding of elementary tactile features during active whisker sensation. Nat Neurosci 12:792–800.
Kaas JH, Nelson RJ, Sur M, Lin CS, Merzenich MM (1979) Multiple representations of the body within the primary somatosensory cortex of primates. Science 204:521–523.
Kerr JN, de Kock CP, Greenberg DS, Bruno RM, Sakmann B, Helmchen F (2007) Spatial organization of neuronal population responses in layer 2/3 of rat barrel cortex. J Neurosci 27:13316–13328.
Khasabov SG, Truong H, Rogness VM, Alloway KD, Simone DA, Giesler GJ Jr (2020) Responses of neurons in the primary somatosensory cortex to itch- and pain-producing stimuli in rats. J Neurophysiol 123:1944–1954.
Klapoetke NC, Murata Y, Kim SS, Pulver SR, Birdsey-Benson A, Cho YK, Morimoto TK, Chuong AS, Carpenter EJ, Tian Z, Wang J, Xie Y, Yan Z, Zhang Y, Chow BY, Surek B, Melkonian M, Jayaraman V, Constantine-Paton M, Wong GK, et al. (2014) Independent optical excitation of distinct neural populations. Nat Methods 11:338–346.
LaMotte RH, Dong X, Ringkamp M (2014) Sensory neurons and circuits mediating itch. Nat Rev Neurosci 15:19–31.
Liu X, Miao XH, Liu T (2020) More than scratching the surface: recent progress in brain mechanisms underlying itch and scratch. Neurosci Bull 36:85–88.
Ma Q (2010) Labeled lines meet and talk: population coding of somatic sensations. J Clin Invest 120:3773–3778.
Mancini F, Haggard P, Iannetti GD, Longo MR, Sereno MI (2012) Fine-grained nociceptive maps in primary somatosensory cortex. J Neurosci 32:17155–17162.
Milenkovic N, Zhao WJ, Walcher J, Albert T, Siemens J, Lewin GR, Poulet JF (2014) A somatosensory circuit for cooling perception in mice. Nat Neurosci 17:1560–1566.
Mu D, Deng J, Liu KF, Wu ZY, Shi YF, Guo WM, Mao QQ, Liu XJ, Li H, Sun YG (2017) A central neural circuit for itch sensation. Science 357:695–699.
Papoiu AD, Coghill RC, Kraft RA, Wang H, Yosipovitch G (2012) A tale of two itches: common features and notable differences in brain activation evoked by cowhage and histamine induced itch. Neuroimage 59:3611–3623.
Paricio-Montesinos R, Schwaller F, Udhayachandran A, Rau F, Walcher J, Evangelista R, Vriens J, Voets T, Poulet JF, Lewin GR (2020) The sensory coding of warm perception. Neuron 106:830–841.e833.
Parker AJ, Newsome WT (1998) Sense and the single neuron: probing the physiology of perception. Annu Rev Neurosci 21:227–277.
Pei YC, Denchev PV, Hsiao SS, Craig JC, Bensmaia SJ (2009) Convergence of submodality-specific input onto neurons in primary somatosensory cortex. J Neurophysiol 102:1843–1853.
Penfield W, Boldrey E (1937) Somatic motor and sensory representation in the cerebral cortex of man as studied by electrical stimulation. Brain 60:389–443.
Peron SP, Freeman J, Iyer V, Guo C, Svoboda K (2015) A cellular resolution map of barrel cortex activity during tactile behavior. Neuron 86:783–799.
Petersen CC (2019) Sensorimotor processing in the rodent barrel cortex. Nat Rev Neurosci 20:533–546.
Petersen CC, Crochet S (2013) Synaptic computation and sensory processing in neocortical layer 2/3. Neuron 78:28–48.
Petreanu L, Gutnisky DA, Huber D, Xu NL, O'Connor DH, Tian L, Looger L, Svoboda K (2012) Activity in motor-sensory projections reveals distributed coding in somatosensation. Nature 489:299–303.
Ploner M, Schmitz F, Freund HJ, Schnitzler A (2000) Differential organization of touch and pain in human primary somatosensory cortex. J Neurophysiol 83:1770–1776.
Prsa M, Morandell K, Cuenu G, Huber D (2019) Feature-selective encoding of substrate vibrations in the forelimb somatosensory cortex. Nature 567:384–388.
Ran C, Hoon MA, Chen X (2016) The coding of cutaneous temperature in the spinal cord. Nat Neurosci 19:1201–1209.
Sun YG, Zhao ZQ, Meng XL, Yin J, Liu XY, Chen ZF (2009) Cellular basis of itch sensation. Science 325:1531–1534.
Sur M, Wall JT, Kaas JH (1981) Modular segregation of functional cell classes within the post-central somatosensory cortex of monkeys. Science 212:1059–1061.
Wang F, Belanger E, Cote SL, Desrosiers P, Prescott SA, Cote DC, De Koninck Y (2018) Sensory afferents use different coding strategies for heat and cold. Cell Rep 23:2001–2013.
Woolsey TA, Van der Loos H (1970) The structural organization of layer IV in the somatosensory region (SI) of mouse cerebral cortex: the description of a cortical field composed of discrete cytoarchitectonic units. Brain Res 17:205–242.
Yarmolinsky DA, Peng Y, Pogorzala LA, Rutlin M, Hoon MA, Zuker CS (2016) Coding and plasticity in the mammalian thermosensory system. Neuron 92:1079–1092.